

INTERSTRATIFICATION IN EXPANDABLE MICA PRODUCED BY CATION-EXCHANGE TREATMENT

HIROSHI TATEYAMA,¹ HIROAKI NOMA,¹ SATOSHI NISHIMURA,¹ YOSHIO ADACHI,¹ MASARU OOI² AND KAZUO URABE³

¹ Kyushu National Industrial Research Institute, Shuku-machi, Tosu city, Saga Prefecture, 841 Japan

² CO-OP Chemicals Co. Ltd, 1-23-3, Chiyoda-ku, Tokyo, 102, Japan

³ Department of Applied Chemistry, School of Engineering, Nagoya University, Furo-cho, Chikusa-ku, Nagoya, 464, Japan

Abstract—A unique interstratified expandable mica was obtained by cation exchange treatments using an expandable mica synthesized from talc. The ²³Na magic angle spinning (MAS) nuclear magnetic resonance (NMR) spectrum of the expandable mica used as a starting material showed that it had 2 kinds of Na⁺: one was exchangeable and the other was not exchangeable. Half of the Na⁺ per unit cell of the expandable mica was replaced with Mg²⁺ by cation exchange treatments. The X-ray powder diffraction (XRD) analysis of the Mg²⁺-exchanged expandable mica, after heating at 73 °C, indicated that Na⁺ in the interlayer sheets was exchanged with Mg²⁺ in every second layer and that it had an interstratified structure with a 12.5-Å layer thickness and a 9.6-Å layer thickness. The structure of the Mg²⁺-exchanged expandable mica was changed into a unique interstratified structure by the calcination at 600 °C; one component had a stacking sequence of talc and a small amount of OH⁻, but the other had a different stacking sequence from talc and no structural OH⁻.

Key Words—¹H MAS NMR Spectra, ²³Na, ²⁹Si, Cation Exchange, Interstratification, Migration.

INTRODUCTION

The interstratification in clay minerals is very important and is an interesting theme both in studying the alteration process in geological problems (Bailey 1988) and synthesizing a new functional material as a technological approach (Guan et al. 1988; Guan and Pinnavaia 1994; Bagshaw and Cooney 1995). Guan et al. (1988) succeeded in synthesizing a novel pillared clay using an interstratified clay (rectorite). The thermal and hydrothermal stabilities of pillared rectorite were much better than those of the usual pillared clay. The other type of interstratified pillared clay was synthesized using montmorillonite (Singh and Kodama 1988) and one of our authors, Urabe et al. (1993, 1996), also succeeded in synthesizing the interstratified pillared clay using an expandable mica.

Expandable micas, such as NaMg_{2.5}Si₄O₁₀F₂ and LiMgLiSi₄O₁₀F₂, generally have a positive charge deficiency in the octahedral sites and alkali ions with a small ionic radius in the interlayer sites. One of the characteristic properties of expandable micas is that they swell in the water like montmorillonite. Shell and Ivey (1969) and Daimon (1978) synthesized these swellable micas from the mixture of Na₂O-MgO-MgF₂-SiO₂ or Li₂O-MgO-MgF₂-SiO₂ melted at 1300–1500 °C. Tateyama et al (1990, 1992, 1996) also synthesized the expandable mica from talc using an intercalation procedure.

Urabe et al. (1993, 1996) reported that the pure interstratified pillared clay could only be obtained from the expandable mica synthesized by the intercalation procedures. In their report, half of the Na⁺ in the ex-

pandable mica was exchanged with Mg²⁺ in the Mg(NO₃)₂ solutions, and the ion-exchanged mica was calcined at 600 °C. The calcined sample was mixed with water and acetone and an aluminum hydroxyl cluster cation solution was added to the suspension. The interstratified pillared clay was obtained after the calcination at 300 °C. If we can know the interstratification mechanism of the expandable mica by ion-exchange treatments, other kinds of novel pillared clays can be synthesized using this expandable mica. The aim of the present paper is, therefore, to study the interstratification process of the expandable mica by cation exchange treatments.

EXPERIMENTAL METHODS

An expandable mica used as a starting material was synthesized using talc and Na₂SiF₆ as follows. The talc used in this study was from the Kanshi deposit in China, and the Na₂SiF₆ used was a reagent-grade chemical. The 1-*M* talc, Mg₃Si₄O₁₀(OH)₂, and the 0.4-*M* Na₂SiF₆ were mixed and milled in a vibrating ball mill. The mixture was heated at 800 °C for 2 h in an electric furnace. The synthetic product consisted mainly of an expandable mica and very small amounts of cristobalite. Each 1.5 g of the expandable mica was dispersed in 150 mL of an aqueous 0.002–0.1-*M* Mg(NO₃)₂ solution (Table 1). After standing for 24 h with stirring, the expandable mica was washed 6 times with 100 mL of the distilled water by centrifugation and some of them were calcined at 600 °C for 3 h. The symbols for each sample are shown in Table 1.

Table 1. Experimental conditions of samples.

	Expandable mica (g)	MgNO ₃ (M)	Temperature (°C)
M-1H	1.5	0.0020	600
M-2H	1.5	0.0025	600
M-3H	1.5	0.0030	600
M-4H	1.5	0.0035	600
M-4N	1.5	0.0035	20
M-5H	1.5	1.00	600

Chemical analyses of the products were carried out by X-ray fluorescence analysis with an accelerating voltage of 55 kV and a current of 50 mA based on the fundamental parameter methods (Rigaku 3270 spectrometer). The thermal gravimetric (TG)-differential thermal gravimetric (DTG) curves were simultaneously recorded upon heating 30 mg of each sample from room temperature to 250 °C at a heating rate of 10 °C/min using a Perkin Elmer TGA-7. The Fourier transform infrared (FTIR) absorption spectra were recorded with a Perkin Elmer FTIR-1760X, using the KBr disk method. The XRD patterns of the samples were measured on a Philips APD-15 using graphite-monochromatized CuK α radiation by the step-scanning technique. The XRD analyses with a heating apparatus were carried out with a Rigaku RAD X-ray diffractometer using a graphite monochromator, and the heating rate was 0.5 °C/min. The ²⁹Si NMR spectra were obtained under the conditions of high-power decoupling magic angle spinning (HD-MAS) and cross polarization magic angle spinning (CP-MAS) at ambient temperature using a Bruker AC200 spectrometer with a Bruker MAS probe tuned to silicon at a frequency of 39.765 MHz. The samples were packed into zirconia double air-bearing rotors which required 0.5 g of powder, and the sample spinning rates were 3.3 kHz. The ²⁹Si spectra were recorded using a repetition time of 5 s for the cross-polarization experiments and 120 s without cross-polarization after 1024 and 360 scans using 90 pulses, respectively. The ¹H MAS NMR spectra were also recorded on the Bruker AC200 using a repetition time of 5 s and 18 scans. The ²³Na spectra were obtained using a Bruker DSX 300 with a repetition time of 4 s and 1024 scans, and the sample spinning rates were 12 kHz.

RESULTS

The chemical composition, structural formula and cation exchange capacity (CEC) of the expandable mica used as the starting material are summarized in Table 2. The structural formula for half a unit cell was calculated on the basis of 22 positive and negative charges. The chemical compositions and structural formulae of the expandable mica, in which Na⁺ was partly ion-exchanged with Mg²⁺, are shown in Table 3. The Na⁺ in the interlayer sheets decreased with the

Table 2. Chemical composition, structural formula and CEC of expandable mica as a starting material.

(A) Chemical composition (wt%)							
SiO ₂	Al ₂ O ₃	Fe ₂ O ₃	MgO	CaO	Na ₂ O	K ₂ O	F
58.2	0.3	0.06	26.8	0.1	5.0	0.01	9.6
(B) Structural formula							
Na _{0.66} Mg _{2.70} (Si _{3.95} Al _{0.02} Mg _{0.03})O _{10.06} F _{1.88}							
(C) CEC (meq/100 g) [†]							
84.9							

[†] Measured by Schöllenger and Simon's method (1945).

increasing concentration of Mg²⁺ from M-1H to M-5H. In the present report, the samples of M-4N and M-4H are focused on because half of the exchangeable Na⁺ in the interlayer sheets of the expandable mica was exchanged with Mg²⁺.

The TG and DTG curves of M-4N are shown in Figure 1. Three-step dehydrations occurred; the first weight loss from room temperature to 90 °C was 3.6 wt%, the second one from 90 °C to 120 °C was 5.3 wt%, and the third one from 120 °C to 250 °C was 2.1 wt%. If we assume that the weight loss below 90 °C represents the adsorbed water on the surface of the expandable mica, the residual weight loss (7.4 wt%) becomes the dehydration of the interlayer water.

The XRD pattern of the expandable mica is shown in Figure 2A. The expandable mica had a monolayer hydrate with a layer thickness of 12.5 Å and did not show any evidence of interstratification in the XRD

Table 3. Chemical compositions, structural formulae of Mg²⁺-exchanged expandable micas. M-1H to M-5H: Analyzed after heating at 600 °C (see Table 1).

(A) Chemical compositions (wt%)									
	SiO ₂	Al ₂ O ₃	Fe ₂ O ₃	MgO	CaO	Na ₂ O	K ₂ O	F	H ₂ O
M-1H	59.1	0.3	0.06	28.4	0.1	3.2	0.01	8.8	—
M-2H	59.2	0.3	0.06	28.6	0.1	2.9	0.01	8.8	—
M-3H	59.3	0.3	0.06	28.9	0.1	2.6	0.01	8.7	—
M-4H	59.4	0.3	0.06	29.1	0.1	2.3	0.01	8.7	—
M-4N [†]	55.0	0.3	0.06	26.9	0.1	2.1	0.01	8.1	7.4
M-5H	59.6	0.3	0.06	29.9	0.1	1.4	0.01	8.6	—
(B) Structural formulae									
M-1H	(Na _{0.42})(Mg _{0.12} Mg _{2.70})(Si _{3.95} Al _{0.02} Mg _{0.03})O _{10.14} F _{1.71}								
M-2H	(Na _{0.38})(Mg _{0.14} Mg _{2.70})(Si _{3.95} Al _{0.02} Mg _{0.03})O _{10.14} F _{1.71}								
M-3H	(Na _{0.34})(Mg _{0.16} Mg _{2.70})(Si _{3.95} Al _{0.02} Mg _{0.03})O _{10.15} F _{1.69}								
M-4H	(Na _{0.30})(Mg _{0.18} Mg _{2.70})(Si _{3.95} Al _{0.02} Mg _{0.03})O _{10.16} F _{1.68}								
M-5H	(Na _{0.20})(Mg _{0.23} Mg _{2.70})(Si _{3.95} Al _{0.02} Mg _{0.03})O _{10.17} F _{1.67}								

[†] The value of H₂O (wt%) was obtained from TG-analysis in the text and the chemical composition was calculated on the basis of the data for M-4H.

[‡] Number of Mg²⁺ migrated into the octahedral sheets and calculated using the following equation: Mg²⁺ (Migrated ion) = Mg²⁺ (Total) - Mg²⁺ (Octahedral sheet) - Mg²⁺ (Tetrahedral sheet).

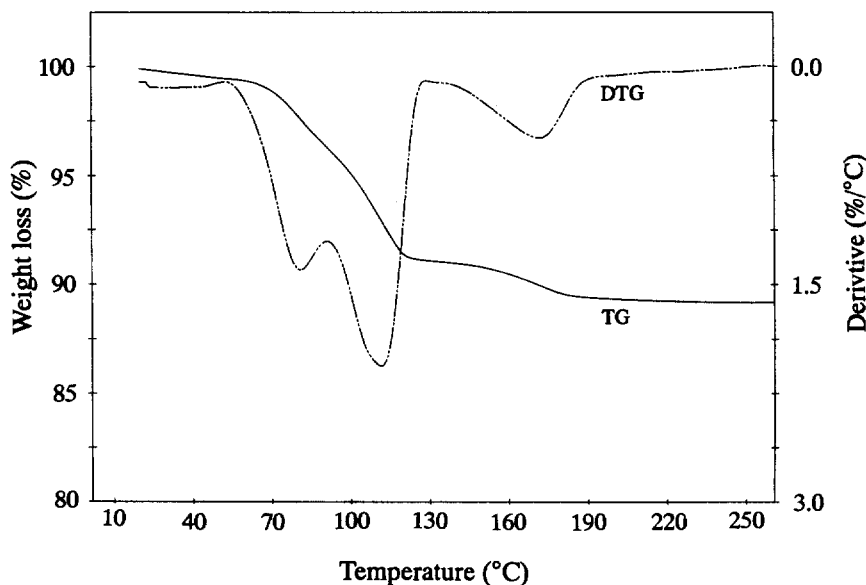


Figure 1. TG and DTG curves of M-4N.

patterns. The XRD patterns of M-4N obtained at different elevated temperatures are shown in Figures 2B to 2E. In the XRD pattern, Figure 2B, this specimen exhibited a weak peak at 27.6 Å and a strong peak at 14.2 Å at 20 °C. The weak peak at 27.6 Å may be ascribed to the regular interstratification of a 15.1-Å layer and a 12.5-Å layer, and the strong peak at 14.2 Å can be explained by the random interstratification of these 2 layers. Figure 2C shows that the strong peak at 14.2 Å shifted to 13.4 Å at 27 °C and that the peak at 13.4 Å did not shift any more up to 33 °C, which indicates that the peak at 13.4 Å also showed the random interstratification of the 15.1-Å layer and the 12.5-Å layer. The 2 new broad peaks at 22.1 Å and at 12.5 Å appeared at 33 °C as shown in Figure 2D. These 2 peaks were assumed to be the reflection of the interstratification of the 12.5-Å layer and the 9.6-Å layer which was estimated from an observed layer thickness of the expandable mica heated at 600 °C, but there was some possibility that the peak at 12.5 Å was overlapped with the peak assigned to the mica containing monolayer hydrate. In Figure 2E, the peak at 13.4 Å disappeared and the 2 peaks at 22.1 and 11.6 Å were only recognized at 73 °C, which indicates that the 2 peaks can be ascribed to the interstratification of the 12.5-Å layer and the 9.6-Å layer, as will be explained later. Figure 3 shows the XRD pattern of M-4N heated at 600 °C (M-4H), which was very similar to that of the talc, but the observed $d(001)$ value (9.45 Å) was larger than that (9.35 Å) of the talc used.

The ^{29}Si HD-MAS NMR spectrum of the expandable mica showed 1 relatively broad peak at -95.1

ppm, but M-4H had 2 peaks at -96.2 and -99.1 ppm, as shown in Figure 4. These 3 peaks were assigned to the Q^3 Si sites of the SiO_4 tetrahedrons with 3 bridged oxygen atoms and 1 nonbridged oxygen. The IR spectra of the expandable mica and M-4H are shown in Figure 5. In Figure 5A, the absorption bands at 996 and 471 cm^{-1} can be assigned to the in-plane Si-O stretching and bending vibrations, respectively, and the 2 other bands at 1082 and 700 cm^{-1} can be assigned to the perpendicular Si-O stretching vibrations on the basis of the theoretical calculations and the assignments of the synthetic Al-free magnesium micas (Tateyama et al. 1976) and the assignments of fluor-talc (Perez and Burlitch 1995). After calcination at 600 °C, Figure 6B, the in-plane Si-O stretching absorption band at 996 cm^{-1} shifted to a peak at 1046 cm^{-1} with a shoulder peak at 1023 cm^{-1} .

Figure 6 shows the ^{29}Si CP-MAS NMR spectra of the expandable mica and M-4H. The ^{29}Si CP-MAS spectrum of the expandable mica as shown in Figure 6A did not show any peaks. On the contrary, in the ^{29}Si CP-MAS spectrum of M-4H, a sharp peak was present at -98.9 ppm along with an upfield signal at about -96 ppm as shown in Figure 6B. The ^1H MAS NMR spectrum of M-4H was measured as shown in Figure 7. The 2 peaks at 3.9 and 1.0 ppm were observed in the ^1H MAS NMR spectrum. The broad peak at 3.9 ppm can be assigned to the ^1H of water molecules bound to Na^+ because the intensity of the peak at 3.9 ppm decreased with decreasing Na^+ from M-1H to M-5H. The sharp peak at 1.0 ppm was very close to that (0.7 ppm) of the talc. The intensity of this peak increased with increasing Mg^{2+} from M-1H to M-5H.

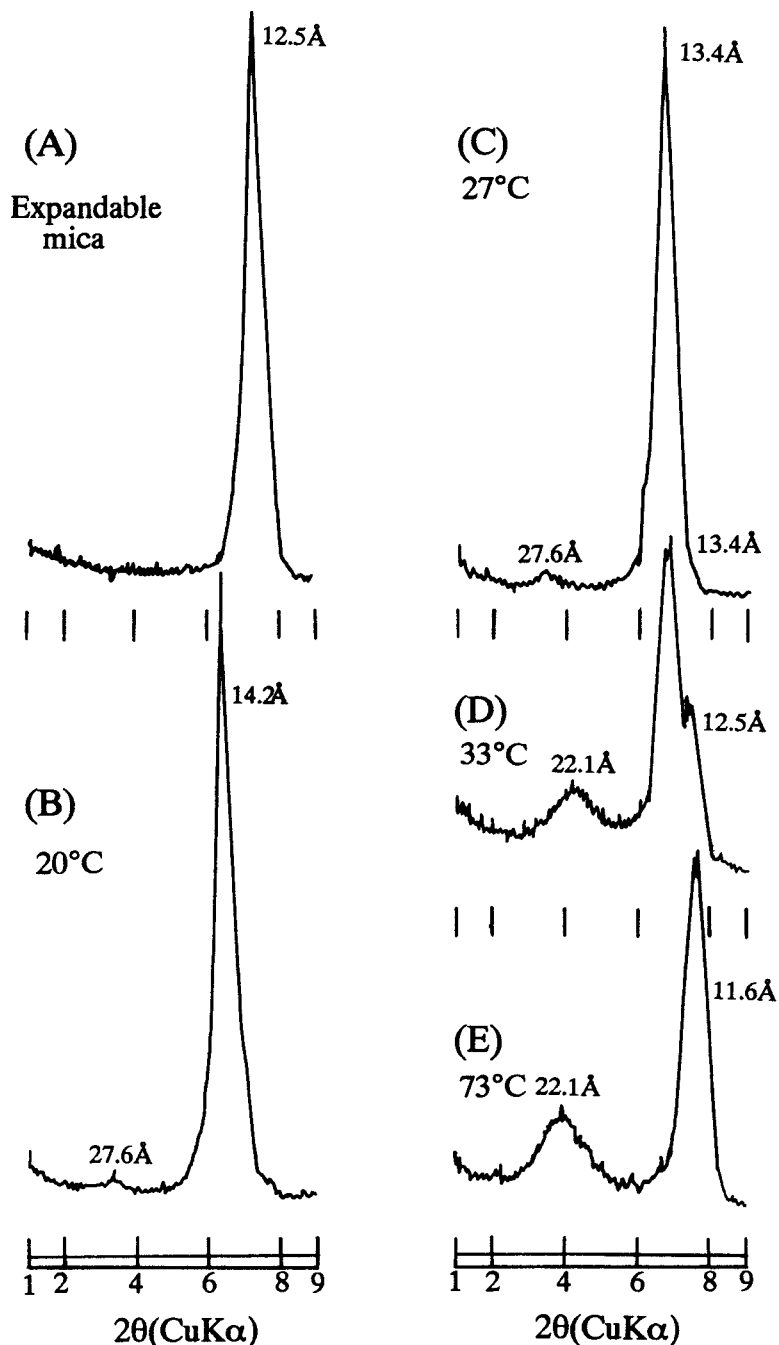


Figure 2. XRD patterns of expandable mica and M-4N heated at different elevated temperatures.

The ^{23}Na MAS NMR spectrum of the expandable mica in Figure 8A showed 2 kinds of signals: one was a sharp peak at 43 ppm in the range of 0–50 ppm and the other was a series of signals in the –100 to 0 ppm range with a wide band-width. The ^{23}Na MAS NMR spectrum of the expandable mica was similar to that

of Na-tetrasilicic mica (Soma et al. 1990). The ^{23}Na MAS NMR spectrum of M-4N showed that the intensity of one strong sharp peak was almost constant, but that of the peak with a wide bandwidth became weak as shown in Figure 8B. Figure 8C shows the ^{23}Na MAS NMR spectrum of M-4H. The sharp peak at 34

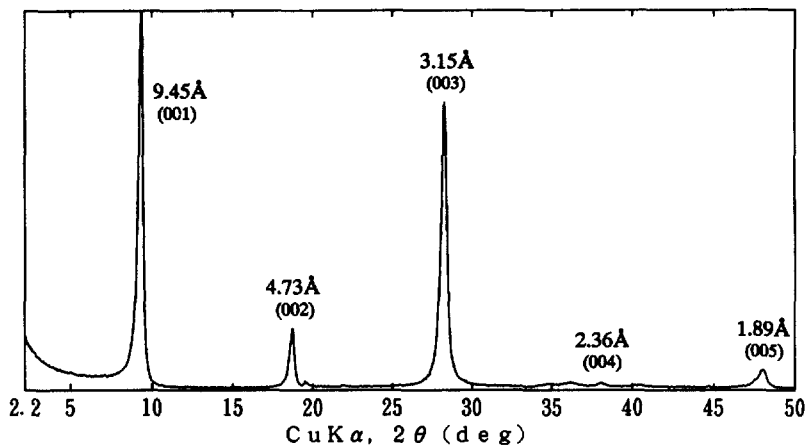


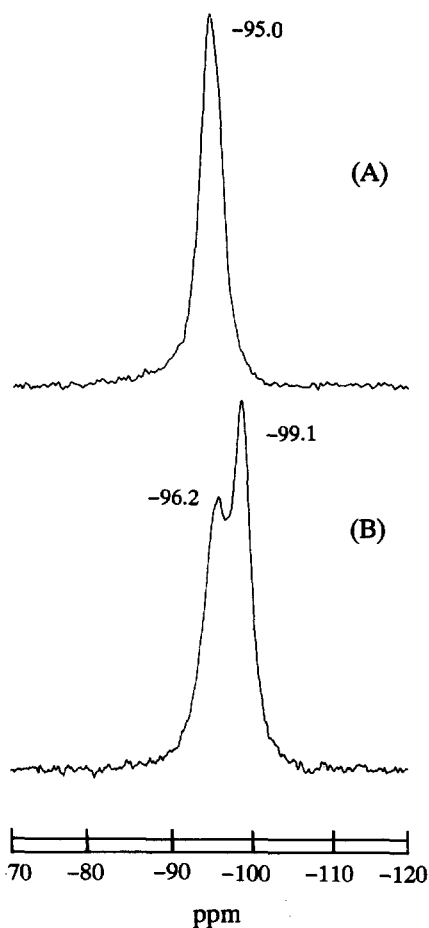
Figure 3. XRD pattern of M-4H.

ppm became very weak and shifted toward the sharp peak at -23 ppm.

DISCUSSION

Interstratified Structure at Low Temperature (73 °C)

In order to confirm the interstratification of M-4N, the XRD profiles of the interstratified structure were calculated on the basis of the Hendricks and Teller equation (1942). The calculation procedures followed the method of Sato (1987, 1988). The XRD pattern of M-4N showed that it consisted of the mixture of regular and random interstratified structures. It was difficult to refine the structure of M-4N, but the M-4N, after heating at 73 °C, changed into a pure interstratified structure (M-4X). Therefore, the XRD profile of M-4X was calculated based on the structural model as shown in Figure 9, in which one component has the 12.5 -Å layer thickness and the other has the 9.6 -Å layer thickness. The structural model of M-4X is explained in detail later in each paragraph. Figure 10 shows the calculated XRD profiles of the interstratified structure based on the above model. The XRD profile in Figure 10A was calculated on the basis of Reichweite (R) = 1 using parameters such as W_{M1} (existence probability of the 12.5 -Å layer) = 0.60, W_{N0} (existence probability of the 9.6 -Å layer) = 0.40, and P_{M1-N0} (continuing probability of these 2 layers) = 0.99. Figure 10B shows the calculated XRD profile of the interstratified structure which has the regularly ordered one because of the same existence probabilities ($W_{M1} = 0.5$ and $W_{N0} = 0.5$). Figure 10C shows the calculated XRD profile of the interstratified structure, in which it has different existence probabilities ($W_{M1} = 0.40$ and $W_{N0} = 0.60$). The observed pattern of Figure 2E was close to that of the calculated profile of Figure 10A. This result indicated that M-4X had the regularly interstratified structure, but the existence probability of one component (12.5 -Å layer) was slightly larger than that of the other component (9.6 -Å layer).

Figure 4. ^{29}Si HD-MAS NMR spectra of expandable mica (A) and M-4H (B).

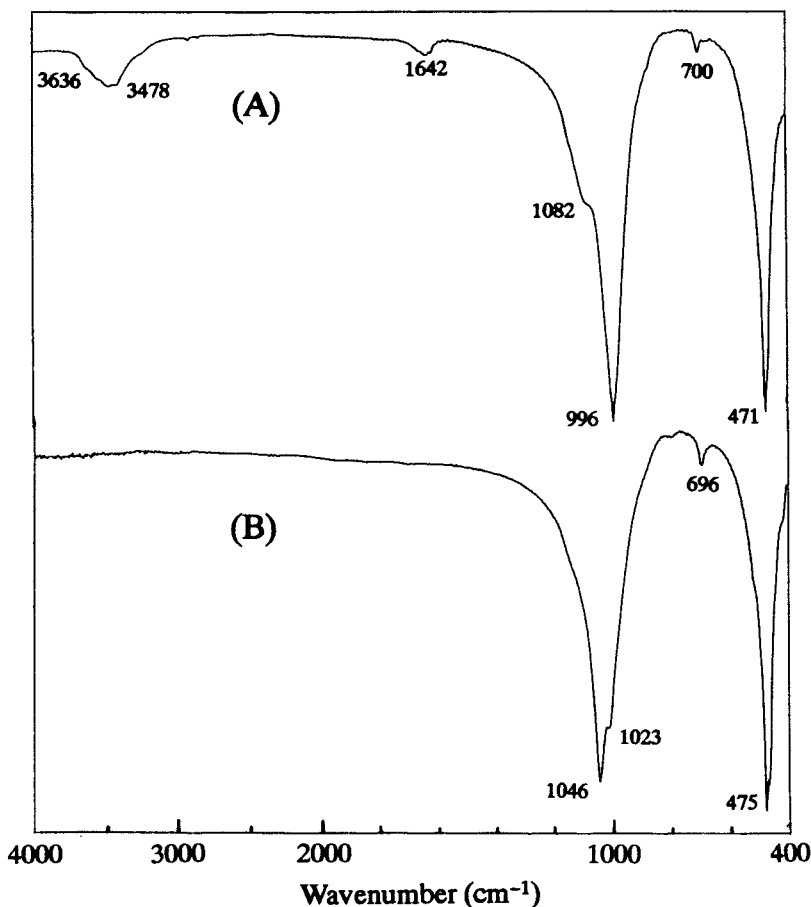


Figure 5. Infrared absorption spectra of expandable mica (A) and M-4H (B).

Suquet et al. (1975) reported that the transition from the monolayer hydrate to the dehydrated state of Na-saponite occurred at the relative humidity of p/p_0 at 0.1, but the dehydrated state of Mg-saponite was not obtained under a very low relative humidity pressure close to zero. This fact showed that the monolayer hydrate bound to Mg^{2+} was very stable compared to that bound to Na^+ under the very low relative humidity conditions. On the basis of the above relative humidity controlled experiments (Suquet et al. 1975), the third weight loss of M-4N on TG-DTG analysis was assigned to the dehydration of the monolayer bound to Mg^{2+} . The value (2.1 wt%) of the third weight loss was very close to the ideal value (2.4 wt%) of the monolayer per unit cell, which can be expressed as $(Na_{0.6}Mg_{0.3}H_2O)Mg_{5.4}Si_8O_{20}F_4$. These results indicate that M-4X had the interstratified structure of the 2:1 silicate layer with the monolayer hydrate bound to Mg^{2+} and the 2:1 silicate layer having Na^+ with the dehydrated layer. The structural formulae of the 2 components of the interstratified M-4X for a half unit cell were assumed as follows; one component was $(Mg_{0.3}H_2O)Mg_{2.7}Si_4O_{10}F_2$ and the other was

$Na_{0.6}Mg_{2.7}Si_4O_{10}F_2$. From now on the 2 components are denoted as the hydrated Mg-2:1 layer in which Mg^{2+} and water molecules are placed between the top and bottom tetrahedral sheets and the dehydrated Na-2:1 layer in which Na^+ is placed between the top and bottom tetrahedral sheets as shown in Figure 9. Therefore, M-4N originally had the interstratified structure of hydrated Mg-2:1 layer and hydrated Na-2:1 layer, in which the number of water molecules in each layer changed with increasing the temperature from 20 to 73 °C. Why M-4N consists of 2 different layers, such as the Mg-2:1 layer and the Na-2:1 layer, is an interesting point.

We postulated that the interstratification of M-4N had some correlation with the exchangeable properties of the expandable mica, and then an attempt was to completely exchange the Na^+ in the expandable mica using the highly concentrated $MgNO_3$ solutions (1 M). However, all the Na^+ in the expandable mica could not be exchanged with Mg^{2+} as shown in Table 3 (M-5N), which suggested that the expandable mica included nearly 28% nonexchangeable Na^+ in the structure. The ^{23}Na NMR spectra of the expandable mica

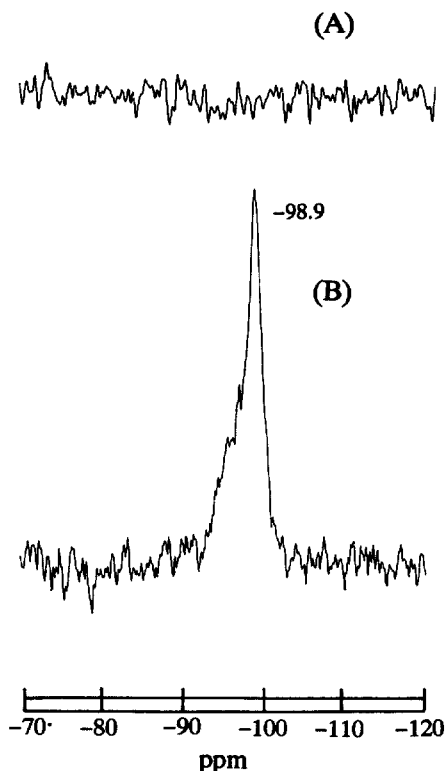


Figure 6. ^{29}Si CP-MAS NMR spectra of expandable mica (A) and M-4H (B).

also supported the above results because the intensity of the peak with a wide bandwidth decreased with increasing Mg^{2+} and the peak disappeared completely at high Mg^{2+} concentration; however, the intensity of the sharp peak at 34 ppm was constant and independent of the Mg^{2+} -exchange treatments. Therefore, the peak with a wide bandwidth can be assigned to the exchangeable Na^+ , and the other sharp signal can be assigned to the exchangeable Na^+ . These results showed that the present expandable mica had 2 different kinds of Na^+ ; one was exchangeable and the other was non-exchangeable. The area ratio of the sharp peak at 34 ppm to the peak with a wide bandwidth was 1:3, which indicated that expandable mica included about 25% nonexchangeable Na^+ in the structure. The ratio of nonexchangeable Na^+ (28 wt%) obtained from chemical analysis was fairly close to that calculated from the ^{23}Na NMR spectra. These results showed that the Na^+ in the one component of the expandable mica was irreversibly fixed in the hexagonal cavities; therefore, it was very difficult to exchange all of the Na^+ in the interlayer sheets. However, the Na^+ in the other component was not fixed tightly in the hexagonal cavities, so it was easy to exchange all of the Na^+ with Mg^{2+} . Therefore, the tetrahedral sheets in the hydrated Mg-2:1 layer had high layer charge and CEC as compared

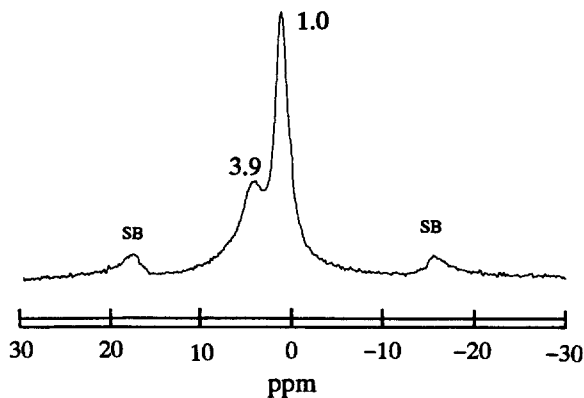


Figure 7. ^1H MAS NMR spectrum of M-4H.

with those in the Na-2:1 layer, which indicated that the M-4X consisted of the 2 different tetrahedral sheets as shown in Figure 9.

Interstratified Structure at High Temperature (600 °C)

The XRD pattern of M-4N heated at 600 °C (M-4H) showed that the $d(001)$ value (9.45 Å) was nearly the average thickness of a 9.35-Å layer thickness of the talc and a 9.60-Å layer thickness of the expandable mica heated at 600 °C. The structural model of M-4H is schematically shown in Figure 11, in which M-4H had the interstratified structure of a calcined Mg-2:1 layer having a 9.35-Å layer thickness and a calcined

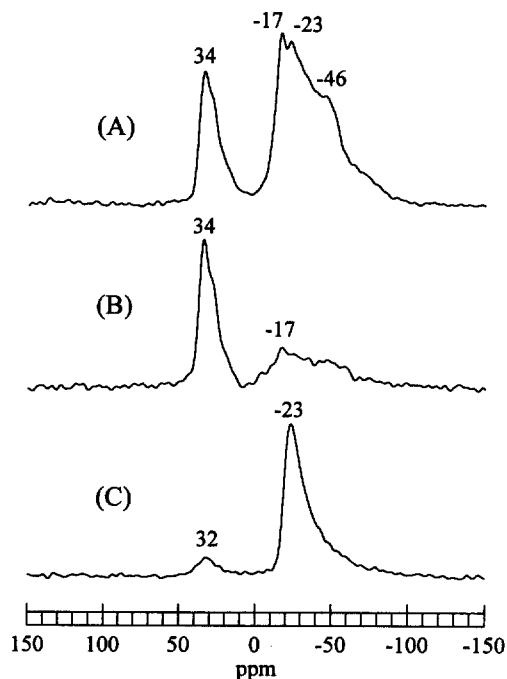


Figure 8. ^{23}Na MAS NMR spectra of expandable mica (A), M-4N (B) and M-4H (C).

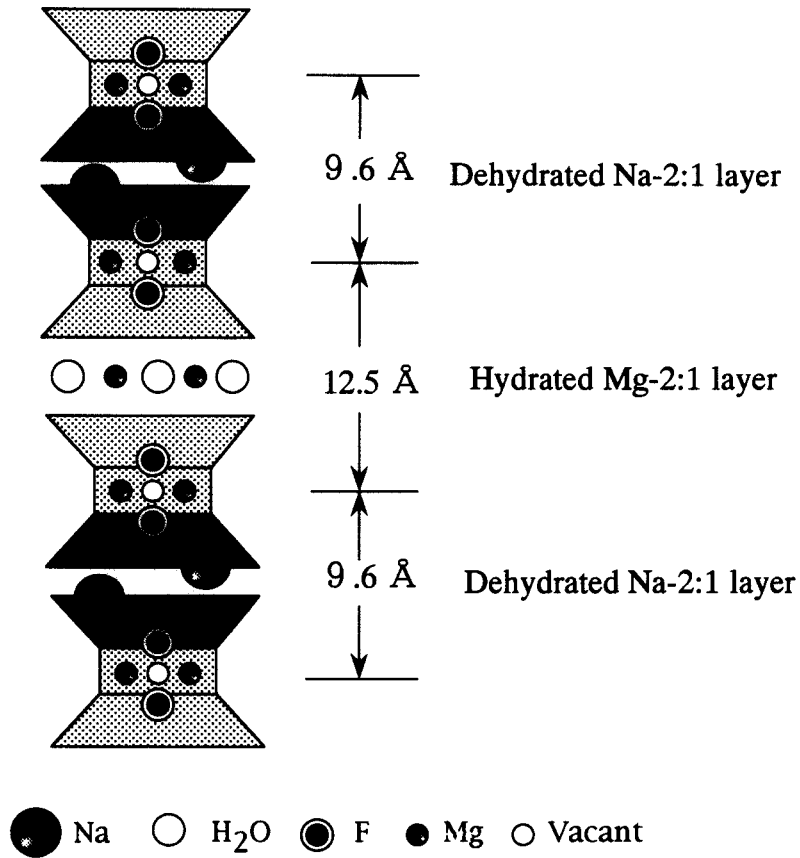
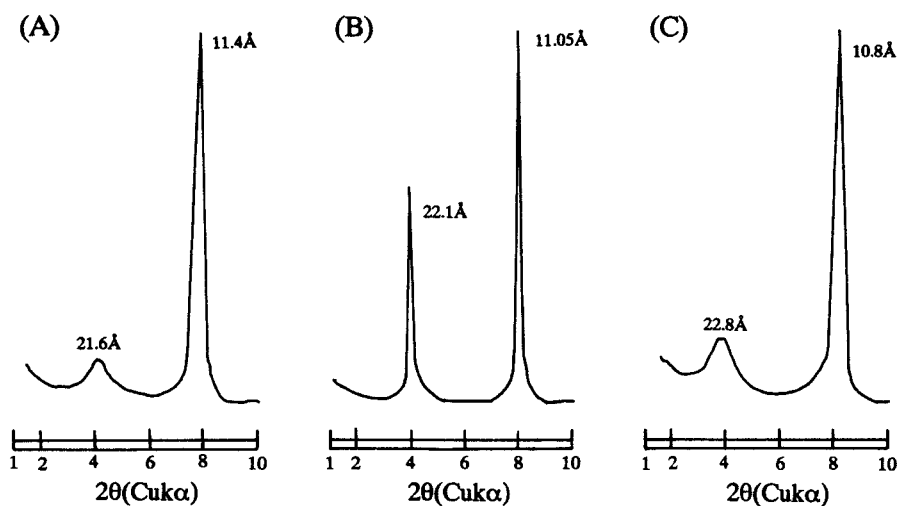


Figure 9. Schematic structural model of M-4X.

Figure 10. XRD profiles of M-4X calculated on the basis of $R = 1$: (A) $W_{N0} = 0.40$, $W_{M1} = 0.60$, $P_{M1-N0} = 0.99$; (B) $W_{N0} = 0.50$, $W_{M1} = 0.50$, $P_{M1-N0} = 0.99$; (C) $W_{N0} = 0.60$, $W_{M1} = 0.40$; $P_{M1-N0} = 0.99$.

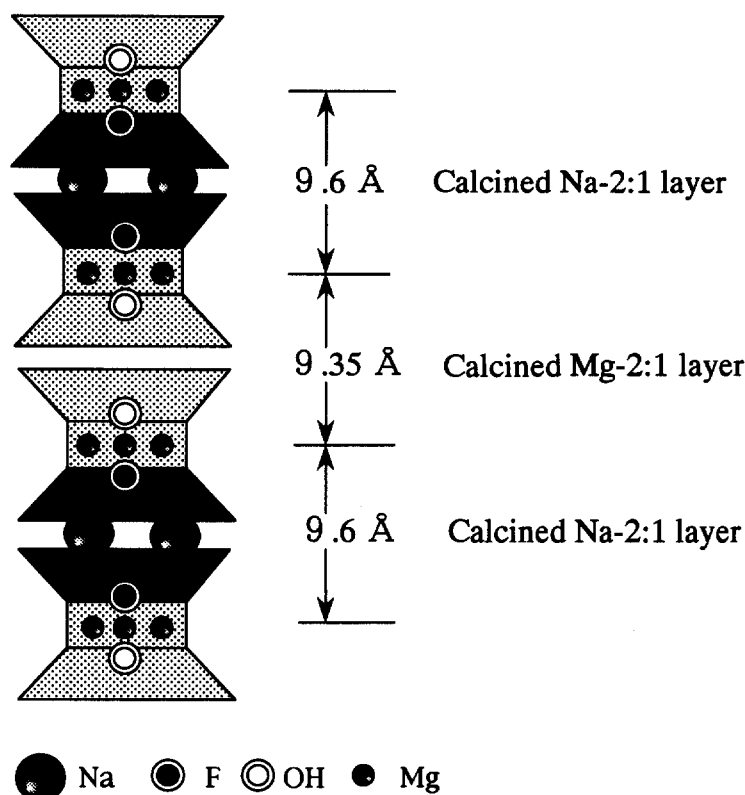


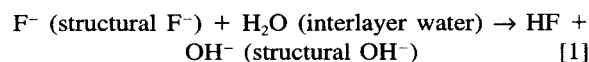
Figure 11. Schematic structural model of M-4H.

Na-2:1 layer having a 9.60-Å layer thickness. The structural model is discussed in detail later based on the results of NMR and FTIR analyses. The 2 signals of the ^{29}Si HD-MAS NMR spectrum and the 2 Si-O stretching bands of the FTIR spectrum of M-4H were considered to show that there were the 2 crystallographically inequivalent Si sites. It is impossible, however, to determine the 2 different sites of the Si atoms without the crystallographic analysis for this sample. Recently, fluoride-substituted talc was synthesized using a sol-gel method under hydrothermal conditions (Perez and Burlitch 1995). They reported that the main absorption band of the Si-O stretching bands for the fluor-talc was 1040 cm^{-1} . Therefore, the absorption band at 1046 cm^{-1} of M-4H can be assigned to the Si-O stretching band of the calcined Mg-2:1 layer, because it was very close to the band at 1040 cm^{-1} of fluor talc. The other absorption band at 1023 cm^{-1} may be assigned to the Si-O stretching band of the calcined Na-2:1 layer. The Si-O stretching band of the expandable mica was 996 cm^{-1} as shown in Figure 6. The shift of the Si-O stretching band from 996 to 1023 cm^{-1} indicated that the network structure of tetrahedral sheets in the Na-2:1 layer was changed by the calcination at $600\text{ }^\circ\text{C}$.

The ^{29}Si chemical shift at -99.1 ppm of M-4H can be assigned to the Q^3 Si sites of the calcined Mg-2:1 layer, because the signal at -99.1 ppm was also close to that (-98.1 ppm) of natural talc (Tateyama et al. 1992). The difference in the ^{29}Si MAS NMR spectrum between the calcined Mg-2:1 layer and the talc may result from the substitution of F^- by OH^- in the talc structure, which means that the calcined Mg-2:1 layer has very low layer charge. This assumption was also supported by Engelhardt and Michel results (1987), in which the decreasing the silicon net charge causes lower frequency shifts on the ^{29}Si NMR spectra. These results clearly indicated that the dehydrated Mg-2:1 layer had a stacking sequence of the talc structure between the 2 tetrahedral sheets, which indicated that, on the calcination at $600\text{ }^\circ\text{C}$, Mg^{2+} in the Mg-2:1 layer of M-4N migrated into the vacant octahedral sheets via the hexagonal cavities in the tetrahedral sheets because of the small ionic radius. The migration of small cations into the vacant octahedral sites of montmorillonite and expandable micas has already been discussed by many authors (Tettenhorst 1962; Farmer and Russell 1967; Tennakoon et al. 1986, 1987; Sakurai et al. 1990). Therefore, the caclined Mg-2:1 layer had no cations in the interlayer sheets.

The ^{29}Si chemical shifts at -95.0 and -96.2 ppm of the expandable mica and M-4H can be also assigned to the Q^3 Si sites of the hydrated and calcined Na-2:1 layer. The lower chemical shifts from -95.0 to -96.2 ppm indicated that the layer charge of the Na-2:1 layer was also reduced by the calcination. However, the 2 tetrahedral sheets of the calcined Na-2:1 layers are not supposed to have the same stacking sequence as talc, because Na^+ is unable to diffuse into the vacant octahedral sites due to the large ionic radius. If the calcined Na-2:1 layer has a mica-like stacking sequence, Na^+ lies centrally on the line joining the centers of the hexagons formed by the basal oxygens of the tetrahedral sheets, and no lateral displacement is introduced going from the basal oxygens of one composite sheet to the corresponding oxygens of its neighbor. On the contrary, the major feature of the talc structure appears to be related to the minimization of the Si^{4+} to Si^{4+} repulsive forces across the interlayer region (Zvyagin et al. 1969). In this arrangement, Si^{4+} is not superimposed over the other Si^{4+} across the interlayer as in the micas (Bailey 1984). It is very difficult to determine the stacking sequence of the calcined Na-2:1 layer, but the stacking sequence of the calcined Na-2:1 layer should be different from that of the calcined Mg-2:1 layer.

In the ^{29}Si CP-MAS spectrum of M-4H, the signal at -96.1 ppm corresponding to the calcined Na-2:1 layer became very weak, but the signal at -98.9 ppm corresponding to the calcined Mg-2:1 layer was clearly observed, as shown in Figure 6. If the silicon atoms are close to the protons, the signal is enhanced with respect to the silicon atoms further from the protons, but the rapid motion of the ^1H can seriously reduce the ^{29}Si - ^1H dipolar interactions (Farnan et al. 1987; Leonardelli et al. 1992). Therefore, the ^1H in the calcined Mg-2:1 layer occupied certain positions in the hexagonal cavities closing to the Si atoms; then the signal at -98.9 ppm appeared very clearly. This assumption was confirmed by the ^1H NMR spectrum, because the sharp signal of the ^1H NMR spectrum was observed at 1.0 ppm, which was very close to the observed signal (0.7 ppm) corresponding to ^1H of the hydroxyl ions in the talc structure. A part of the structural F^- in the calcined Mg-2:1 layer may, therefore, be substituted by the structural OH^- ions when Mg^{2+} diffused into the vacant octahedral sites passing through the hexagonal cavities of the Mg-2:1 layer by the dehydration process as follows:



This assumption was roughly confirmed by the structural formula of M-4H as shown in Table 3, because there were some F^- deficiencies in the structural formula. These results indicated that the calcined Mg-2:1 layer had a small amount of OH^- that partially sub-

stituted F^- in the octahedral sheets as shown in Figure 11.

On the contrary, if protons do not occupy certain positions in the structure, the intensity of the signal at -96.1 ppm should be weak. Therefore, the weak intensity of the signal at -96.1 ppm may show that the Na-2:1 layer does not have any OH^- in the hexagonal cavities. The properties of Na^+ in the interlayer sheets of the hydrated Na-2:1 layer was also different from that of the calcined Na-2:1 layer, because the ^{23}Na MAS NMR spectra of M-4N and M-4H showed that the intensity of the signals at 34 ppm corresponding to the nonexchangeable Na^+ decreased very drastically and shifted to -23 ppm corresponding to the exchangeable Na^+ , which indicated that the Na^+ in the Na-2:1 layer moved from nonexchangeable to exchangeable sites by the calcination at 600°C . The reason for the movement of Na^+ may be the fact that the electrostatic force attracting Na^+ to the hexagonal cavities becomes weak, because the total negative charge of each silicate layer was reduced by the migration of Mg^{2+} into the vacant octahedral sheets. Therefore the calcined Na-2:1 layer had exchangeable Na^+ in the interlayer sheets and no structural OH^- as shown in Figure 11.

CONCLUSIONS

Half of Na^+ of the expandable mica was exchanged with Mg^{2+} by cation exchange treatments using aqueous $3.5 \times 10^{-3} \text{ M Mg}(\text{NO}_3)_2$ solutions. The Mg^{2+} -exchanged expandable mica (M-4N) was heated at different temperatures from 20 to 73°C in order to investigate the interstratification process of the expandable mica. The ^{23}Na MAS NMR spectrum of the expandable mica used as a starting material showed that it had 2 kinds of Na^+ ; one was exchangeable and the other was nonexchangeable. The XRD, NMR and TG-DTG analyses of M-4N indicated that it had the following interstratified structure; one component had the Mg^{2+} that replaced exchangeable Na^+ in the interlayer sheets and the other had a nonexchangeable Na^+ in the interlayer sheets.

Upon heating at 600°C (M-4H), the Mg^{2+} and Na^+ in the interlayer sheets of each layer showed very characteristic properties in the structure. M-4H had a unique interstratified structure which consisted of a calcined Mg-2:1 layer and a calcined Na-2:1 layer as follows: In the calcined Mg-2:1 layer, the Mg^{2+} in the interlayer sheets migrated into the octahedral vacant sites passing through the hexagonal cavities due to the dehydration process. A part of the structural F^- in the calcined Mg-2:1 layer was substituted with OH^- when the Mg^{2+} migrated into the octahedral vacant sites. Therefore the calcined Mg-2:1 layer had the same stacking sequence as talc, no interlayer cations and a small amount of OH^- . On the contrary, in the calcined Na-2:1 layer the Na^+ could not migrate into the hex-

agonal cavities due to the large ionic size, but could move from nonexchangeable to exchangeable sites because of partial neutralization of the layer charge. Therefore, the calcined Na-2:1 layer had a different stacking sequence from talc, the exchangeable Na⁺ and no structural OH⁻.

ACKNOWLEDGMENTS

The writers would like to thank M. Sato of Gunma University for using the program to calculate the XRD profile of the interstratified structure and K. Yamamoto of Fukuoka Agricultural Research Center for measuring the CEC values of the expandable micas.

REFERENCES

- Bagshaw SA, Cooney RP. 1995. Preparation and characterization of a highly stable pillared clay: GaAl12-pillared rectorite. *Chem Mater* 7:1384–1389.
- Bailey SW. 1984. Crystal chemistry of the true micas. In: Bailey SW, editor. *Micas*. Washington DC: Mineral Soc Am p 13–60.
- Bailey SW. 1988. Mixed layer chlorite minerals. In: Bailey SW, editor. *Hydrous phyllosilicates*. Washington DC: Mineral Soc Am p 601–630.
- Daimon N. 1978. Synthetic micas with ultra fine powder. *Sci Am* 8:9–19.
- Engelhardt G, Michel D. 1987. High-resolution solid-state NMR of silicate and zeolite. New York: J. Wiley. p 122–134.
- Farmer VC, Russell JD. 1967. Infrared absorption spectrometry in clay studies. *Clays Clay Miner* 15:121–142.
- Farnan I, Kohn SC, Dupree R. 1987. A study of the structural role of water in hydrous silica glass using cross-polarization magic angle spinning NMR. *Geochim Cosmochim Acta* 49:769–777.
- Guan J, Min E, Yu Z. 1988. Highly stable cross-linked rectorite product—A novel type of cracking catalyst. In: Phillips MJ, Tewnran M, editors. *Chem Inst Can Ottawa Ont. Proc Int Congr Catal. vol I*. p 104–111.
- Guan J, Pinnavaia TJ. 1994. A pillared rectorite clay with highly stable supergalleries. *Mater Sci Forum*: 109–114.
- Hendricks S, Teller E. 1942. X-ray interference in partially ordered layer lattices. *J Chem Phys* 10:147–167.
- Leonardelli S, Facchini L, Fretigny C, Tougne P, Legrand AP. 1992. Silicon-29 nuclear magnetic resonance study of silica. *J Am Chem Soc* 114:6412–6418.
- Perez FD, Burlitch JM. 1995. Sol-gel synthesis of fluoride-substituted talc. *Chem Mater* 7:2277–2283.
- Sakurai H, Urabe K, Izumi Y. 1990. Pillared tetrasilic mica catalysts modified by fixed interlayer cations. Classification of fixation mode by cations. *Bull Chem Soc Jpn* 63:1389–1395.
- Sato M. 1987. Interstratified (mixed layer) structures and their theoretical X-ray powder patterns. I. Theoretical aspects. *Clay Sci* 7:1–48.
- Sato M. 1988. Interstratified (mixed layer) structures and their theoretical X-ray powder patterns. II. In the case of illite/montmorillonite interstratification. *Clay Sci* 7:3–88.
- Schöllenger CJ, Simon RH. 1945. Determination of exchange capacity and exchangeable bases in soils. *Soil Sci* 58:13–25.
- Shell HR, Ivey KH. 1969. Fluorine micas. *US Bur Mines Bull* 647:1–2910.
- Singh SS, Kodama H. 1988. Reactions of polynuclear hydroxyaluminum cations with montmorillonite and the formation of a 28-Å pillared complex. *Clays Clay Miner* 36:397–402.
- Soma M, Tanaka A, Seyama H, Hayashi S, Hayamizu K. 1990. Bonding states of sodium in tetrasilic sodium flour mica. *Clay Sci* 8:1–8.
- Suquet H, Calle CD, Pezerat H. 1975. Selling and structural organization of saponite. *Clays Clay Miner* 23:1–9.
- Tateyama H, Nishimura S, Tsunematsu K, Jinnai K, Adachi Y, Kimura M. 1992. Synthesis of expandable fluorine mica from talc. *Clays Clay Miner* 40:180–185.
- Tateyama H, Shimoda S, Sudo T. 1976. Infrared absorption spectra of synthetic Al-free magnesium micas. *N Jb Miner Mh H3*:128–140.
- Tateyama H, Tsunematsu K, Hirose H, Kimura K, Furusawa T, Ishida Y. 1990. Synthesis of the expandable fluorine mica from talc and its colloidal properties. In: Farmer VC, Tardy Y, editors, *Proc 9th Int Clay Conf Strasbourg. vol II*. p 128–140.
- Tateyama H, Tsunematsu K, Noma H, Adachi Y. 1996. Formation of expandable mica from talc using intercalation procedures. *J Am Ceram Soc* 79:3321–3324.
- Tennakoon DTB, Jones W, Thomas JM. 1987. Characterization of clay and pillared clay catalysis. *Solid State Ionics* 24:205–212.
- Tennakoon DTB, Thomas JM, Jones W, Carpenter TA, Ramdas S. 1986. Characterization of clays and clay-organic systems. *J Chem Soc Faraday Trans I* 82:545–562.
- Tettenhorst R. 1962. Cation migration in montmorillonites. *Am Mineral* 47:769–773.
- Urabe K, Kenmoku I, Izumi Y. 1996. Staging control in microporous pillared clay. *J Phys Chem Solids* 95:1037–1041.
- Urabe K, Kenmoku I, Kawabe K, Izumi Y. 1993. Acidity-tunable pillared micas catalyst derived from talc. *Proc 10th Int Cong Catalyst* 19–24.
- Zvyagin BB, Mischchenko KS, Soboleva SV. 1969. Structure of pyrophyllite and talc in relation to the polytypes of mica-type minerals. *Soviet Phys Cryst* 13:511–515.

(Received 30 May 1996; accepted 8 September 1997; Ms. 2771)